Thin Solid Films xxx (2014) xxx–xxx

Contents lists available at ScienceDirect

Thin Solid Films

journal homepage: www.elsevier.com/locate/tsf

Effects of deposition termination on $Cu_2ZnSnSe_4$ device characteristics

I.L. Repins [a,*], J.V. Li [a], A. Kanevce [a], C.L. Perkins [a], K.X. Steirer [a], J. Pankow [a], G. Teeter [a], D. Kuciauskas [a], C. Beall [a], C. Dehart [a], J. Carapella [a], B. Bob [b], J.-S. Park [a], S.-H. Wei [a]

[a] National Renewable Energy Laboratory, Golden, CO 80401, USA
[b] Department of Materials Science and Engineering, University of California, Los Angeles, CA 90095, USA

ARTICLE INFO

Available online xxxx

Keywords:
Copper zinc tin selenide
Copper zinc tin sulfide
Kesterite
Thin films
Surface
Hole barrier
Voltage
Solar cell

ABSTRACT

Co-evaporated $Cu_2ZnSnSe_4$ (CZTSe) is used to examine sensitivities to the device performance that originate from variations in Zn content very near the surface. While integral Zn content of the film is held approximately constant, the surface composition is manipulated via changes to the Zn flux at the end of the deposition. Surface composition, device performance, and open-circuit voltage extrapolated to zero temperature are measured as a function of deposition termination. Origins of the apparent reduction in surface recombination with increasing Zn are discussed.

1. Introduction

Kesterite devices have made rapid progress, with champion efficiencies reaching 12.6% [1], compared to 6.7% just 6 years ago [2]. However, improvement to near 20% is needed to achieve cost goals associated with terawatt-scale production [3]. Furthermore, even champion devices exhibit voltages that are well below those expected from the measured bulk lifetimes, from 2 to 16 ns [4,5]. Thus, a careful study of possible sources of voltage loss is necessary to achieve the goals of this technology.

In this work, we examine sensitivities to the device performance that originate from the region very near the surface, which may not be characterized by optical or electrical techniques that penetrate further into the film. We use co-evaporated $Cu_2ZnSnSe_4$ (CZTSe) to demonstrate the critical importance of the deposition termination (i.e., the fluxes comprising the top ~500 Å of the film) on device efficiency. The Zn-terminated depositions have produced the highest-published IEC-certified efficiency for a CZTSe device without alloying for bandgap expansion (efficiency, $\eta = 9.8\%$; open-circuit voltage, $V_{oc} = 380$ mV; fill factor, FF = 68.9%; short-circuit current, $J_{sc} = 37.6$ mA/cm^2) [6]. Such devices benefit from reduced surface recombination without experiencing the current-blocking behavior that would be associated with a pure ZnSe surface layer.

2. Experimental

2.1. Film growth

The device structure and growth of the co-evaporated kesterite absorber has been described in an earlier publication [7]. In brief, the device stack was formed by using a soda-lime glass (SLG) substrate, sputtered Mo back contact, 150 Å e-beam-evaporated NaF precursor, four-source co-evaporated CZTSe on 500 °C substrate, chemical-bath-deposited (CBD) CdS, sputtered resistive/conductive ZnO bi-layer, e-beam-evaporated Ni/Al grids, and photolithographic device isolation. No antireflective coating was applied to the devices in this study.

This paper explores several deposition variations that are illustrated schematically in Fig. 1, which shows deposition flux and temperature profiles for CZTSe film growth. Two types of variations in the Zn flux are used in this study. In the first variation, there are two different times for termination of the Zn flux, as shown by the hash-marked portion of the Zn profile. When the Zn flux is terminated before the Cu flux (first hashed line), there is a period of growth where the instantaneous Cu/Zn flux ratio is Cu-rich. When the Zn flux is terminated at the same time as the Cu flux (second hashed line), the instantaneous Cu/Zn flux ratio is always Zn-rich (i.e., <2). In the second variation, excess Zn is applied while the sample is cooling. Two ways of applying excess Zn are shown as black dotted lines. In the first case, where excess Zn is applied at around 35 min, the sample is at high temperature (>430 °C) during the excess Zn deposition. In the second case, where excess Zn is applied at around 50 min, the sample is at low temperature (between 275 °C and 300 °C) during the excess Zn deposition. In a third case, no excess Zn was used to terminate the deposition. In this paper, these

* Corresponding author at: National Renewable Energy Laboratory, 16253 Denver West Pkwy, Golden, CO 80401-3305, USA.
E-mail address: Ingrid.repins@nrel.gov (I.L. Repins).

http://dx.doi.org/10.1016/j.tsf.2014.09.028

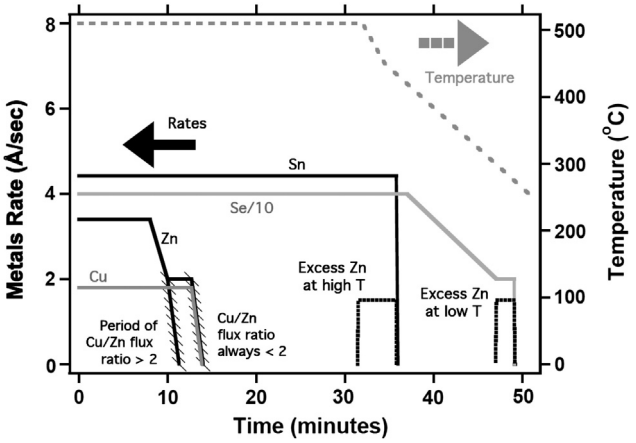

Fig. 1. Deposition rate (left axis) and temperature (right axis) setpoints as a function of time for absorbers in this study. Terminating Zn cap, shown by the black dotted lines, was included in some depositions and omitted in others. Hash marks show options for terminating the Cu rate when instantaneous flux is either Cu-rich or Zn-rich.

cases of excess Zn applied during sample cooling will be referred to as "high-temperature Zn cap," "low-temperature Zn cap," and "no Zn cap," respectively. In each variation, the initial Zn rate is adjusted so that the integral Zn content of each film is similar, around Cu/Zn = 1.3 (Cu/Zn = 2.0 is a stoichiometric CZTSe film). The relationship between instantaneous flux ratios and integral composition has been illustrated in an earlier publication [8]. The flux profiles shown in Fig. 1 are a schematic representation of the rate setpoint. Actual rates are read by electron impact emission spectroscopy beam flux monitor, as described more fully in previous work [7].

2.2. Film characterization

Integral composition of CZTSe films was measured via X-ray fluorescence (XRF) using a Solar Metrology System SMX unit. The XRF measurements were calibrated by inductively coupled plasma optical emission spectroscopy (ICP-OES) performed by Balazs NanoAnalysis. XRF measurements on SLG/Mo substrates measure some amount of Sn from the float glass, even though the Mo is deposited on the non-float side. Thus, the model for interpreting the XRF signal corrects for an assumed constant contribution of the glass to the Sn emission.

X-ray photoelectron spectroscopy (XPS) was performed in a cluster tool that has been described previously [9]. XPS derived compositions were determined using the Cu 3p, Zn 3d, Sn 4d, and Se 3d core levels. Spectra were obtained using non-monochromatic Mg Kα radiation and with a pass energy of 11.75 eV. Satellite subtraction and data analysis were performed within the MultiPak v9.0 software package and used literature sensitivity factors. Prior to analysis, samples were rinsed with de-oxygenated de-ionized water in the glove-box portion of the cluster tool and introduced into the vacuum system without air exposure. Water rinsing removes sodium oxides, which are found in substantial amounts on the surface of our films.

2.3. Device characterization

External quantum efficiency (QE) was measured using an Oriel IQE 200 system. Current–voltage (JV) measurements were performed under AM1.5 conditions. The intensity of an Oriel 81291-1000 W xenon arc lamp was calibrated using a Si reference cell. The sample was placed on a 25 °C cold chuck, and four-point probing (i.e., Kelvin configuration) was used in conjunction with a Keithley 2400 source-measure unit to avoid effects of contact resistance. Short-circuit currents were normalized to the AM1.5-integrated QE values, minus 5% grid coverage, to correct for small (<10%) nonuniformities in simulator illumination and changes in overall intensity calibration.

V_{oc}(T) characteristics were measured by an Agilent B2912A source-measurement unit with the devices illuminated by a Newport 96000 solar simulator. The devices were mounted in a cryo-chamber whose temperature was varied from 70 to 310 K by a closed-cycle-helium refrigerator CTI-22C. A Si diode sensor DT-670 directly attached to the CZTSe film was used to measure the temperature of the device.

3. Results

The samples used in this study and the associated variations on Zn flux are summarized in the first five columns of Table 1. The samples are listed in order of the most Zn expected near the surface, to the least Zn expected near the surface, as based on deposition conditions. The expectation for near-surface Zn is based on two physically reasonable assumptions: First, it is assumed that more Zn will remain in the near-surface region (rather than diffusing throughout the film) when the Zn cap is applied at a lower temperature. Second, it is assumed that—for samples with the same Zn cap—there will be more Zn in the near-surface region if the Cu rate was terminated while the instantaneous Cu/Zn flux ratio was Zn-rich rather than Cu-rich. The fifth column in Table 1 shows the integral Cu/Zn ratio as measured by XRF. All samples are Zn-rich (i.e., Cu/Zn < 2), and there is no trend in integral Zn content of the films as one proceeds down the list.

The atomic percentages of each constituent element at the surface, as measured by XPS, are shown in columns six through nine of Table 1. Several trends are apparent. First, the percentage of Zn measured by the XPS (at the surface) on average decreases as one progresses down the list, as expected from the deposition conditions. Second, it should be noted that all the surfaces are significantly Zn-rich, as a stoichiometric CZTSe sample consists of 25% Cu, 12.5% Zn, and 12.5% Sn, and 50% Se. Even for the two samples where the last metal flux applied was Cu (samples F and G), the Zn content is greater than the stoichiometric value, and the Cu/Zn ratio at the surface is well under the integral value, consistent with previously-observed tendency of the surface to stabilize in a Zn-rich configuration. Third, for samples where some Cu appears at the surface, the surface is enriched in Sn compared to Cu, i.e., the atomic ratio Cu/Sn is significantly less than the stoichiometric value of around two expected for a kesterite. Thus, once cannot interpret the surface to be a simple mixture of pure CZTSe and ZnSe grains, as such a mixture must still yield Cu/Sn around two.

A summary of JV parameters for each absorber is shown in columns 10–13 of Table 1. These parameters are extracted from the JV curves shown in Fig. 2. Several trends are apparent in the JV data. A striking feature of the data is that only the sample with Zn cap deposited at low temperature (A) exhibits the photocurrent-blocking-type behavior [10,11] that would be expected from depositing hundreds of angstroms of ZnSe on top of the absorber [12]. All the samples *except* A exhibit several percent Cu and Sn at the surface that have interdiffused with the Zn. This interdiffusion must change the electronic behavior of this ZnSe-like surface layer, based on the lack of a blocking barrier for all samples except A. Indeed, density functional theory (DFT) predicts that the incorporation of Sn into ZnSe will lower the conduction band edge, because the ZnSe conduction-band minimum derives from an antibonding cation s and anion s hybridized state, and the Sn atom is both larger and more electronegative than Zn. The interdiffusion of small percentages of Cu, Sn, and Zn at high deposition temperatures and associated lack of blocking behavior can explain why ZnS(e) has been reported to exist in fairly large amounts in some devices with apparently little detriment to the device performance [13,14].

A second trend apparent from Fig. 2 is that V_{oc} decreases with Zn content at the surface. For sample A, the FF and J_{sc} are controlled by the blocking behavior of the front ZnSe. However, for samples B through G, the V_{oc} decrease is also accompanied by smaller (percentage-wise) decreases in FF and J_{sc}. The J_{sc} decrease becomes significant (~50%) for the samples with the least Zn-rich surface.

Please cite this article as: I.L. Repins, et al., Effects of deposition termination on $Cu_2ZnSnSe_4$ device characteristics, Thin Solid Films (2014), http://dx.doi.org/10.1016/j.tsf.2014.09.028

Table 1
Summary of sample types, integral composition, surface composition, and JV parameters.

Sample	Deposition number	Zn cap	Last Cu/Zn ratio	Integral Cu/Zn	XPS Cu (%)	XPS Zn (%)	XPS Sn (%)	XPS Se (%)	V_{oc} (mV)	FF (%)	J_{sc} (mA/cm^2)	η (%)	V_{oc}(T = 0, mV)
A	M3926-21	Low T	Zn-rich	1.1	0	48.1	0.6	51.3	400	45	4.6	0.8	0.91
B	M3866-23[a]	High T	Zn-rich	1.4	6.8	28.8	9.2	55.2	368	66	37	8.9	0.883
C	M3711	High T	Cu-rich	1.3	7.4	30.0	8.5	54.1	324	62	34	7.1	0.865
D	M3970-11	None	Zn-rich	1.5	10.7	21.7	12.0	55.7	314	63	30	6.0	0.785
E	M4000-21	None	Zn-rich	1.2	10.2	22.0	11.7	56.1	292	59	32	5.5	0.720
F	M4002-11	None	Cu-rich	1.3	14.6	15.9	13.6	55.9	273	57	24	3.7	0.713
G	M3707	None	Cu-rich	1.5	12.2	21.2	9.6	57.0	266	50	17	2.3	0.674

[a] A piece of the bare absorber was not available from this sample, so another made using the same deposition profile (M3880) was substituted during XPS measurements for this entry.

To further explore the source of the change in the JV parameters, V_{oc} as a function of temperature was measured. The data are shown in Fig. 3. For each sample, a linear fit is used in the range of 250 to 300 K to extrapolate V_{oc}(T) to absolute zero. Temperatures below 250 K were not used in the fit because at certain low temperatures a significant fraction of holes begin to freeze out, changing the position of the Fermi level in the bulk and thus the functional behavior of V_{oc}(T). As one moves from samples A to G, both the fits and the data points for each sample are lower on the graph. Previous publications have discussed the behavior of V_{oc}(T = 0) for differing dominant recombination mechanisms [15,16]. The extrapolations of V_{oc} at T = 0 (i.e. activation energies) are shown in the final column of Table 1. Both V_{oc} and V_{oc}(T = 0) decrease markedly with Zn content at the surface. The relationship between measured sample voltages and activation energies is shown in Fig. 4.

Theory and experiment indicate a bandgap for CZTSe around 1.0 eV [17]. An activation energy value below the bandgap has been associated with interface effects [15,16]. In such cases, the activation energy is the hole barrier, i.e., the distance from the absorber valence band edge to the Fermi level at the interface. When recombination in the bulk is dominant, the activation energy is equal to the bandgap. Thus, one would conclude that the electrical behavior of samples F and G are controlled by defects at the surface, and that the degree of this behavior decreases as the surface is made more Zn-rich.

Although deposition conditions for samples A through G are identical other than the termination, one cannot rule out an effect on V_{oc} from bulk minority-carrier lifetime in the present data. However, even if bulk minority-carrier lifetime affects V_{oc} under AM1.5 conditions, it cannot lead to the activation energy values lower than the bandgap. When activation energy is less than the absorber bandgap, a contribution from the interface must be involved in the form of either a negative conduction-band offset with interface recombination, or Fermi level pinning at the interface [16].

4. Discussion

One can hypothesize four changes that might lead to the observed decrease in surface recombination with increasing Zn, as deduced from V_{oc}(T) data: i) The bandgap has been expanded at the surface via the valence band moving downward in energy. Thus, the hole barrier has been increased by that amount. ii) The surface recombination velocity has been decreased. iii) The conduction-band offset has become more favorable, i.e., we have moved from a "cliff" [18] or nearly flat alignment, to a moderate "spike." iv) The bandgap has increased through the majority of the space-charge region, and thus, V_{oc}(T) indicates a change that is effectively in the bulk.

Several pieces of data and results from theory are relevant to assessing the likelihood of each of the four hypotheses above. First, regarding hypothesis (i) (increase in hole barrier), a continuous and approximately linear increase in the distance between the Fermi level and the valence band edge with increasing Zn content has been documented in other measurements of CZTS. Thus, if surface recombination is important in kesterite devices, it should be strongly influenced by the Zn content at the surface and the associated increase in hole barrier.

There is some basis in theory for the plausibility of hypothesis (ii), reduction in surface recombination velocity. DFT predicts that a Sn-rich surface will exhibit defects near mid-gap, and a Zn-rich one will not [19]. However, all the samples in this study were found to have a very Zn-rich surface. In varying the deposition termination, we simply cause the surface to become *more* Zn-rich. Thus, it seems unlikely that the voltage behavior of this sample set is due mainly to a modification of surface recombination velocity. Furthermore, although surface ecombination velocity affects V_{oc} under operating conditions, V_{oc} at

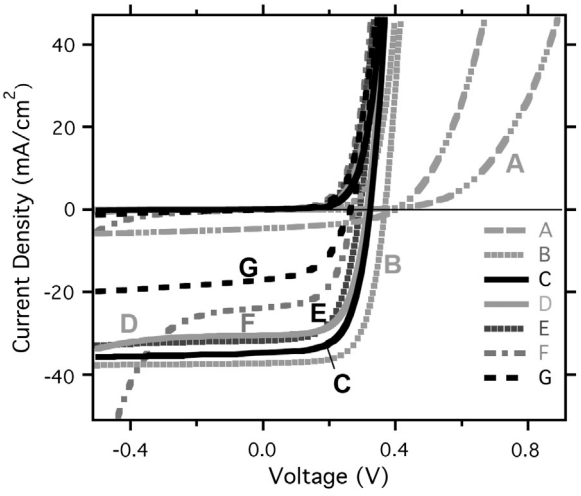

Fig. 2. Light and dark JV curves for devices from Table 1.

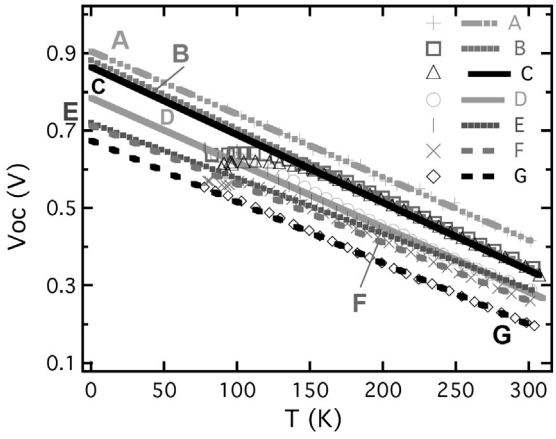

Fig. 3. Open-circuit voltage as a function of temperature for samples of Table 1.

Please cite this article as: I.L. Repins, et al., Effects of deposition termination on $Cu_2ZnSnSe_4$ device characteristics, Thin Solid Films (2014), http://dx.doi.org/10.1016/j.tsf.2014.09.028

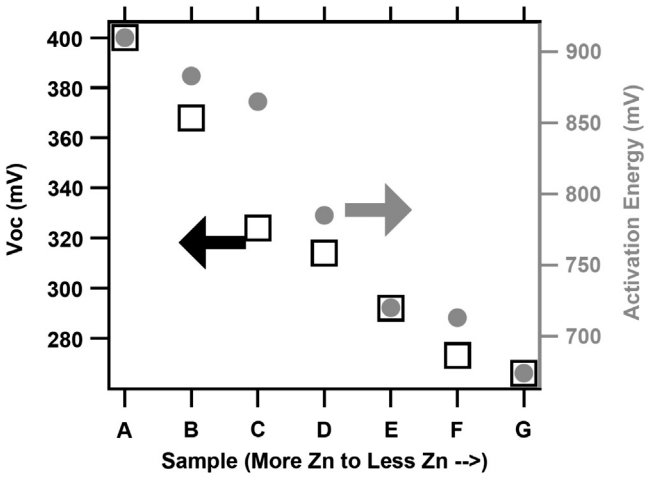

Fig. 4. Open circuit voltage versus extracted activation energy for each sample.

T = 0—which decreases markedly as one progresses down (Table 1)—is a function only of the hole barrier, not the surface recombination velocity [15].

It is possible that creating a more favorable conduction-band offset (hypothesis iii) plays some part in the voltage behavior observed in this study. Independent studies of the electronic surface and interface structures of CdS/CZTSe samples similar to B indeed suggest the presence of a small spike in the conduction band, and a surface gap around 1.2 eV. These results will be reported in separate upcoming publications.

It seems unlikely that hypothesis iv (increase in bulk bandgap) can account for the behavior documented in Table 1. According to rate monitors, about 500 Å of ZnSe is applied, which approximately matches the width of the region of elevated Zn detected in Auger profiles. The depletion width in these devices, on the other hand, is around 0.2 μm [20]. Thus, the region of expanded bandgap is less than half the depletion region thickness. Furthermore, the activation energy value for samples F and G, ~670 mV, is far too low to be controlled primarily by the bulk properties of a material with an expected bandgap of ~1.0 eV [17].

It should be noted that although using a Zn-rich surface termination has been shown to greatly reduce surface recombination and improve performance in CZTSe devices, there is still unexplained voltage loss in kesterite devices. For the best CZTSe device made by the method described in this paper [6], the voltage loss, defined to be V_L = (bandgap − V_{oc}), is V_L = 1000 − 380 = 620 mV. Similarly, for the record 12.6% CZTSS device, V_L = 1130 − 513 = 617 mV. Data on similar or larger voltage loss for CZTSS devices with a variety of S contents can be found in the literature [21,22]. These voltage losses are larger than expected based on a measured minority-carrier lifetime and device modeling [4]. A prediction of voltage loss by luminescence techniques [21] also points to some unexplained loss in the present state-of-the-art devices.

5. Conclusions

In this study, we have shown that a very Zn-rich near-surface layer provides a performance benefit to co-evaporated CZTSe devices. Even when samples are Zn-rich overall, all JV parameters suffer when a Zn-rich termination is not included. V_{oc}(T) data indicate that the impact of surface defects is significantly reduced by the Zn-rich termination. The most likely explanation for the performance benefit seems to be bandgap expansion leading to an increase in the hole barrier, and possibly a more favorable conduction-band alignment. Although the composition of the Zn-rich near-surface region is within several percent of ZnSe, it does not act as a current-blocking barrier when it contains these amounts of Cu and Sn.

Acknowledgments

For surface measurements related to samples in this study, the authors thank M. Bär of Helmholtz-Zentrum Berlin für Materialien und Energie (HZB), J.H. Alsmeier of HZB, L. Weinhardt of University of Nevada at Las Vegas (UNLV) and Karlsruhe Institute of Technology (KIT), D.A. Hanks of HZB and UNLV, R.G. Wilks of HZB, and C. Heske of UNLV and KIT.

This work was supported by the U.S. Department of Energy under Contract No. DE-AC36-08GO28308 with the National Renewable Energy Laboratory.

References

[1] W. Wang, M.T. Winkler, O. Gunawan, T. Gokmen, T.K. Todorov, Y. Zhu, D.B. Mitzi, Device characteristics of CZTSSe thin-film solar cells with 12.6% efficiency, Adv. Energy Mater. 4 (2014) 1301465.
[2] H. Katagiri, K. Jimbo, S. Yamada, T. Kamimura, W.S. Maw, T. Fukano, T. Ito, T. Motohiro, Enhanced conversion efficiencies of Cu_2ZnSnS_4-based thin film solar cells by using preferential etching technique, Appl. Phys. Express 1 (2008) 041201.
[3] M. Le, Tackling challenges in solar: 2014 portfolio, U.S. Government Report Number DOE/EE-1081, May 2014.
[4] I.L. Repins, H. Moutinho, S.G. Choi, A. Kanevce, D. Kuciauskas, P. Dippo, C.L. Beall, J. Carapella, C. DeHart, B. Huang, S.H. Wei, Indications of short minority-carrier lifetime in kesterite solar cells, J. Appl. Phys. 114 (2013) 084507.
[5] T. Gokmen, O. Gunawan, D.B. Mitzi, Minority carrier diffusion length extraction in $Cu_2ZnSn(Se,S)_4$ solar cells, J. Appl. Phys. 114 (2013) 114511.
[6] Certified measurement, NREL device performance group.
[7] I. Repins, C. Beall, N. Vora, C.D. Hart, D. Kuciauskas, P. Dippo, B. To, J. Mann, W.-C. Hsu, A. Goodrich, R. Noufi, Co-evaporated $Cu_2ZnSnSe_4$ films and devices, Sol. Energy Mater. Sol. Cells 101 (2012) 154.
[8] W.-C. Hsu, I. Repins, C. Beall, C. DeHart, B. To, W. Yang, Y. Yang, R. Noufi, Growth mechanisms of co-evaporated kesterite: a comparison of Cu-rich and Zn-rich composition paths, Prog. Photovolt. Res. Appl. 22 (2014) 35.
[9] C.L. Perkins, F.S. Hasoon, Surfactant-assisted growth of CdS thin films for photovoltaic applications, J. Vac. Sci. Technol. A 24 (2012) 497.
[10] A.O. Pudov, A. Kanevce, H.A. Al-Thani, J.R. Sites, F.S. Hasoon, Secondary barriers in CdS–$CuIn_{1-x}Ga_xSe_2$ solar cells, J. Appl. Phys. 97 (2005) 064901.
[11] A.O. Pudov, Impact of Secondary Barriers on $CuIn_{1-x}Ga_xSe_2$ Solar Cell Operation, Ph.D. thesis, Colorado State University, 2005.
[12] J.B. Yoo, A.L. Fahrenbruch, R.H. Bube, Preparation and properties of $CuInSe_2$ solar cells with a ZnSe intermediate layer, Proc. 20th IEEE PVSC, 1988, p. 1431.
[13] N. Vora, J. Blackburn, I.L. Repins, C. Beall, B. To, J. Pankow, G. Teeter, M. Young, R. Noufi, Phase identification and control of thin films deposited by co-evaporation of elemental Cu, Zn, Sn, and Se, J. Vac. Sci. Technol. A 30 (2012) 051201.
[14] K. Wang, B. Shin, K.B. Reuter, T. Todorov, D.B. Mitzi, S. Guha, Structural and elemental characterization of high efficiency Cu_2ZnSnS_4 solar cells, Appl. Phys. Lett. 98 (2011) 051912.
[15] U. Rau, H.W. Schock, Electronic properties of Cu(In, Ga)Se2 heterojunction solar cells—recent achievements, current understanding, and future challenges, Appl. Phys. A 69 (1999) 131.
[16] R. Scheer, Activation energy of heterojunction diode currents in the limit of interface recombination, J. Appl. Phys. 105 (2009) 104505.
[17] S. Chen, A. Walsh, J.H. Yang, X.G. Gong, L. Sun, P.X. Yang, J.H. Chu, S.-H. Wei, Compositional dependence of structural and electronic properties of $Cu_2ZnSn(S,Se)_4$ alloys for thin film solar cells, Phys. Rev. B 83 (2011) 125201.
[18] R. Klenk, Characterisation and modelling of chalcopyrite solar cells, Thin Solid Films 387 (2001) 135.
[19] P. Xu, S. Chen, B. Huang, H.J. Xiang, X.G. Gong, S.-H. Wei, Stability and electronic structure of Cu_2ZnSnS_4 surfaces: First-principles study, Phys. Rev. B 88 (2013) 045427.
[20] J.V. Li, D. Kuciauskas, M.R. Young, I.L. Repins, Effects of sodium incorporation in co-evaporated $Cu_2ZnSnSe_4$ thin-film solar cells, Appl. Phys. Lett. 102 (2013) 163905.
[21] T. Gokmen, O. Gunawan, T.K. Todorov, D.B. Mitzi, Band tailing and efficiency limitation in kesterite solar cells, Appl. Phys. Lett. 103 (2013) 103506.
[22] M.T. Winkler, W. Wang, O. Gunawan, H.J. Hovel, T.K. Todorov, D.B. Mitzi, Optical designs that improve the efficiency of $Cu_2ZnSn(S,Se)_4$ solar cells, Energy Environ. Sci. 7 (2014) 1029.